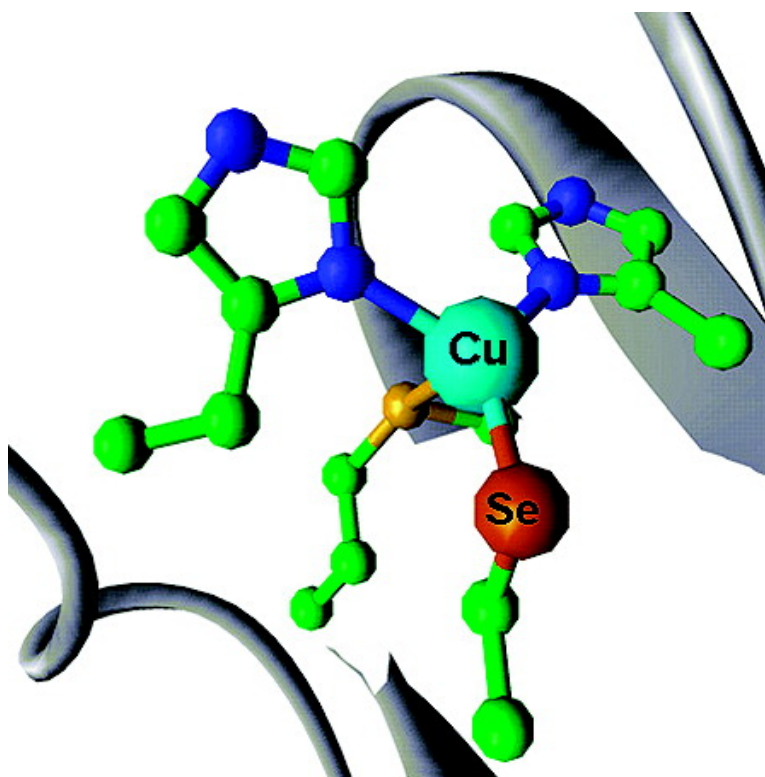Article

The Selenocysteine-Substituted Blue Copper Center: Spectroscopic Investigations of Cys112SeCys *Pseudomonas aeruginosa* Azurin

Martina Ralle, Steven M. Berry, Mark J. Nilges, Matt D. Gieselman,
Wilfred A. van der Donk, Yi Lu, and Ninian J. Blackburn

More About This Article

Additional resources and features associated with this article are available within the HTML version:

- Supporting Information
- Links to the 6 articles that cite this article, as of the time of this article download
- Access to high resolution figures
- Links to articles and content related to this article

ACS Publications
High quality. High impact.

• Copyright permission to reproduce figures and/or text from this article

View the Full Text HTML

The Selenocysteine-Substituted Blue Copper Center: Spectroscopic Investigations of Cys112SeCys *Pseudomonas aeruginosa* Azurin

Martina Ralle,[†] Steven M. Berry,[‡] Mark J. Nilges,[§] Matt D. Gieselman,[‡] Wilfred A. van der Donk,[‡] Yi Lu,[‡] and Ninian J. Blackburn*,[†]

Contribution from the Department of Environmental & Biomolecular Systems, OGI School of Science & Engineering, Oregon Health & Science University, 20000 NW Walker Road, Beaverton, Oregon 97006, and the Department of Chemistry and University of Illinois EPR Research Center (IERC), University of Illinois at Urbana-Champaign, 600 South Mathews Avenue, Urbana, Illinois 61801

Received December 18, 2003; E-mail: ninian@ebs.ogi.edu

Abstract: Azurin is a small electron-transfer protein belonging to the cupredoxin family. The Cu atom is located within a trigonal plane coordinated by two histidines (His46 and His117) and a cysteine (Cys112) with two more distant ligands (Gly45 and Met121) providing axial interactions. A Cys112SeCys derivative has been prepared by expressed protein ligation, and detailed UV/vis, EPR and EXAFS studies at the Cu and Se K-edges have been carried out. Marked changes are observed between the EPR parameters of the Cys112SeCys and WT azurin derivatives, which include a 2-fold increase in $A_{\parallel}$, a decrease in g-values, and a large increase in rhombicity of the g-tensor. The Cu−Se and Se−Cu bond lengths obtained from analysis of the Cu and Se K-EXAFS of the oxidized protein were found to be 2.30 and 2.31 Å, respectively, 0.14 Å longer than the Cu−S distance of the WT protein. Unexpectedly, the Cu−Se bond lengths were found to undergo only minor changes during reduction, suggesting a very similar structure in both redox states and extending the "rack" hypothesis to the Se-substituted protein.

Introduction

Selenium substitution is a powerful ligand-directed technique for determining metalloprotein coordination using X-ray absorption spectroscopy (XAS). Selenomethionine incorporation using methionine auxotrophic cell lines has become widespread for solving crystal structures using MAD techniques, but in general SeMet substitution is global and hence provides little information of value to X-ray spectroscopists on Se−metal interactions since these constitute only a small fraction of the total Se scattering. In cases where few methionine residues are present, Se−metal scattering has been effectively used as a spectral probe of structure. Thus, for example, cytochrome *ba₃* oxidase subunit II contains only one methionine, which is itself a ligand to the Cu_A center,[1] allowing Blackburn and co-workers to probe the copper methionine interaction by both Cu and Se K-EXAFS.[2,3] SeMet substitution of the heme ligand Met80 in cytochrome *c* was achieved by chemical synthesis of peptide fragments followed by autocatalytic fragment religation.[4] Se substitution of substrates has also proved powerful in confirming substrate

binding to metalloprotein active sites: Penner-Hahn and co-workers have provided unambiguous evidence for homocysteine binding to different forms of methionine synthase using a Se-substituted homocysteine substrate.[5]

The most functionally important S-containing metal-binding residue in proteins is cysteine, and selenocysteine (SeCys) incorporation would thus represent a powerful use of Se as a ligand-directed spectroscopic probe of structure and function. Although SeCys is a naturally occurring amino acid found in a growing number of classes of both prokaryotic and eukaryotic enzymes (glutathione peroxidase, thioredoxin reductase, formate dehydrogenase, CO dehydrogenase, certain hydrogenases, deiodinases, and others), the machinery of tRNA loading of SeCys is complex and unsuitable for prokaryotic expression systems.[6−8] An alternative approach is the novel technique of native chemical ligation,[9−11] which involves the thiol-catalyzed condensation of a synthetic peptide carrying an N-terminal Cys residue with a peptide carrying a thioester moiety at the C-terminus to generate a native amide bond. This approach has been used successfully to prepare synthetic protein molecules

---

† Oregon Health & Science University.
‡ Department of Chemistry, University of Illinois at Urbana-Champaign.
§ IERC, University of Illinois at Urbana-Champaign.

(1) Williams, P. A.; Blackburn, N. J.; Sanders, D.; Bellamy, H.; Stura, E. A.; Fee, J. A.; McRee, D. E. *Nat. Struct. Biol.* **1999**, *6*, 509−516.
(2) Blackburn, N. J.; de Vries, S.; Barr, M. E.; Houser, R. P.; Tolman, W. B.; Sanders, D.; Fee, J. A. *J. Am. Chem. Soc.* **1997**, *119*, 6135−6143.
(3) Blackburn, N. J.; Ralle, M.; Gomez, E.; Hill, M. G.; Patsuszyn, A.; Sanders, D.; Fee, J. A. *Biochemistry* **1999**, *38*, 7075−7084.
(4) Wallace, C. J. A.; Clarke-Lewis, I. *J. Biol. Chem.* **1992**, *267*, 3852−3861.

(5) Peariso, K.; Zhou, Z. S.; Smith, A. E.; Matthews, R. G.; Penner-Hahn, J. E. *Biochemistry* **2001**, *40*, 987−993.
(6) Birringer, M.; Pilawa, S.; Flohe, L. *Nat. Prod. Rep.* **2002**, *19*, 693−718.
(7) Stadtman, T. C. *Annu. Rev. Biochem.* **2002**, *71*, 1−16.
(8) Low, S.; Berry, M. J. *Trends Biochem. Sci.* **1996**, *21*, 203−208.
(9) Wilken, J.; Kent, S. B. H. *Curr. Opin. Biotechnol.* **1998**, *9*, 412−426.
(10) Kochendoerfer, G. G.; Kent, S. B. H. *Curr. Opin. Chem. Biol.* **1999**, *3*, 665−671.
(11) Cotton, G. J.; Muir, T. *Chem. Biol.* **1999**, *6*, R247−R256.

containing unnatural or labeled amino acids including fluoro-phoric probes,[12] isotopically labeled domains for NMR,[13,14] and large protein−protein conjugates.[15] It has also been used successfully to incorporate Se-containing amino acids into specific sites in peptides and proteins. Using native chemical ligation strategies, Gieselman and co-workers prepared a 17-mer that corresponded to the C-terminus of ribonucleotide reductase with SeCys in place of Cys.[16] Low and co-workers[17] extended the synthetic strategy by use of a cleavable N-terminal thiol auxiliary group, obviating the need for a Cys residue at the N-terminus of one of the peptide fragments and thus succeeded in incorporating a single SeMet residue as the axial ligand to the heme in cytochrome b_{562}, a protein that contains no cysteine residues. Expressed protein ligation (EPL) is a variant of native chemical ligation in which the peptide fragment containing the C-terminal thioester is produced using an intein fusion vector. Raines and co-workers successfully used this procedure to synthesize a ribonuclease derivative containing SeCys at position 110. Since the C56−C110 disulfide is critical to proper folding and catalytic function, the restoration of native levels of activity after SeCys incorporation elegantly demon-strated the formation of a Cys56−SeCys110 cross-link.[18]

Azurin is a small electron-transfer protein belonging to the cupredoxin family. The Cu atom is located within a trigonal plane by two histidines (His46 and His117) and a cysteine (Cys112) with two additional (more distant) axial ligands, Gly45 and Met121, as depicted in the structure shown in Figure 1. Recently, we reported the use of EPL to construct semisynthetic azurin derivatives made possible by the fact that three of the metal-binding residues are found close to the C-terminus.[19,20] When selenocysteine was used as the N-terminal residue, SeCys was incorporated into the full-length azurin molecule at position 112.[19] We have communicated details of the preparation and initial characterization of this derivative. Of special note is that the potentials of wild-type (WT) and Cys112SeCys azurin were surprisingly similar, given the expected stabilization of Cu(I) by selenolate, which may suggest a compensatory change in geometrical and/or electronic structure. Here we extend our studies on the Cys112SeCys azurin to include detailed EPR and EXAFS studies at the Cu and Se K-edges in both the oxidized and reduced forms and to a derivative containing a double S to Se mutation, Cys112SeCys−Met121SeMet. Unexpectedly, the Cu−Se bond lengths are found to undergo only minor changes during reduction, suggesting a very similar structure in both redox states and extending the "rack" hypothesis to the Se-substituted protein. However, changes in EPR parameters and absorption edge features may suggest some perturbation of the electronic structure at copper. This represents the first
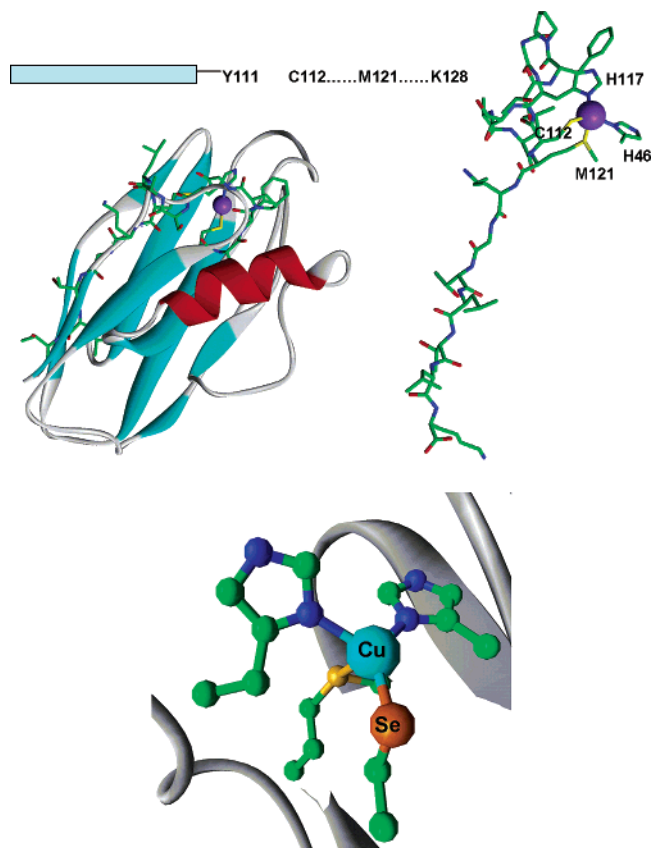

Figure 1. Crystal structure of *P. aeruginosa* azurin (PDB file 4AZU). Top right: active site showing the copper atom, ligand residues His46, Cys112, His117, and Met121, and the 17-mer C-terminal ligated peptide extending from residues Cys112 to Lys128. Top left: the interaction of the synthetic peptide C-terminus with the rest of the molecule. Bottom: expanded view of the expected copper coordination in the SeCys112 derivative.

XAS study in which SeCys substitution has been used to probe metal-site structure in an engineered metalloprotein.

Experimental Section

Gene Construction. The gene fragment corresponding to the first 111 amino acids of *P. aeruginosa* azurin was copied from the WT azurin pET9a plasmid, obtained as a generous gift from Professor John H. Richards. PCR was used to copy the DNA sequence while creating a new SapI site near the coding region for residue 111 of the WT azurin gene. Utilizing the existing NdeI site at the N-terminus of the protein, along with the newly created SapI site, the fragment was digested and ligated into the commercially available pTXB1 vector (New England Biolabs, Beverly, MA).

Peptide Synthesis. Protected amino acids were purchased from either Advanced ChemTech (Louisville, KY) or Chem Impex International, Inc. (Wooddale, IL). Fmoc-protected selenomethionine was synthesized and purified following literature procedures from selenomethionine (Acros) and *N*-(9-fluorenylmethoxycarbonyloxy) succinimide (Fmoc-Osu) (Advanced Chemtech).[21] Se-*p*-methoxybenzyl (PMB) seleno-cysteine was prepared as reported previously.[16] Wang resin preloaded with the C-terminal Fmoc-protected amino acid was obtained from Advanced ChemTech.

The C-terminus of azurin was synthesized on a 0.2 mmol scale with a Rainin model PS3 peptide synthesizer (Rainin Instrument Company, Inc., Woburn, MA) using Fmoc chemistry. Wang resin was swollen in DMF (3 × 6 mL, 10 min). Fmoc deprotection for all amino acids except for Fmoc-SeCys(PMB) was accomplished with 20% v/v piperidine/

(12) Cotton, G. J.; Ayers, B.; Xu, R.; Miur, T. W. *J. Am. Chem. Soc.* **1999**, *121*, 1100−1101.
(13) Otomo, T.; Ito, N.; Kyogoku, Y.; Yamazaki, T. *Biochemistry* **1999**, *38*, 16040−16044.
(14) Xu, R.; Ayers, B.; Cowburn, D.; Muir, T. W. *Proc. Natl. Acad. Sci. U.S.A.* **1999**, *96*, 388−393.
(15) Becker, C. F. W.; Hunter, C. L.; Seidel, R.; Kent, S. B. H.; Goody, R. S.; Englehard, M. *Proc. Natl. Acad. Sci. U.S.A.* **2003**, *100*, 5075−5080.
(16) Gieselman, M. D.; Xie, L.; van der Donk, W. A. *Org. Lett.* **2001**, *3*, 1331−1334.
(17) Low, D. W.; Hill, M. G.; Carrasco, M. R.; Kent, S. B. H.; Botti, P. *Proc. Natl. Acad. Sci. U.S.A.* **2003**, *98*, 6554−6559.
(18) Hondal, R. J.; Nilsson, B. L.; Raines, R. T. *J. Am. Chem. Soc.* **2001**, *123*, 5140−5141.
(19) Berry, S. M.; Gieselman, M. D.; Nilges, M. J.; van der Donk, W. A.; Lu, Y. *J. Am. Chem. Soc.* **2002**, *124*, 2084−2085.
(20) Berry, S. M.; Ralle, M.; Low, D. W.; Blackburn, N. J.; Lu, Y. *J. Am. Chem. Soc.* **2003**, 8760−8768.

(21) Rose, R. B.; Endrizzi, J. A.; Cronk, J. D.; Holton, J.; Alber, T. *Biochemistry* **2000**, *39*, 15062−15070.

DMF (4 × 6 mL, 6 min). The selenocysteine derivative was Fmoc-deprotected with 20% v/v piperidine/DMF only twice for 5 min to minimize complications with deselenation.[22] A 4-fold excess of the amino acids (0.8 mmol) was activated with *O*-benzotriazole-*N,N,N′,N′*-tetramethyluronium hexafluorophosphate (HBTU, 0.8 mmol) and 0.4 M *N*-methylmorpholine (30 s) and coupled to the resin. Each amino acid was coupled for 1 h or until ninhydrin test of the resin indicated the coupling was complete. For SeCys(PMB), a double coupling was performed.

Peptide Cleavage. Wang resin with the peptide attached was washed with DMF (3 × 3 mL), EtOH (3 × 3 mL), and CH_2Cl_2 (3 × 3 mL) and dried in a vacuum desiccator overnight. The dry resin was added to a solution consisting of H_2O (1 mL), anisole (1 mL), thioanisole (1 mL), and TFA (20 mL) at 0 °C and stirred for 1 h. The solvent was then filtered, and the resin was washed with TFA (3 × 3 mL). The TFA was evaporated, and the peptide was precipitated with cold Et_2O. The resulting white solid was isolated by filtration, dissolved in a 1:1 mixture of $MeCN/H_2O$, and lyophilized. The white solid was purified at a preparative scale by reverse-phase HPLC using a Waters (Milford, MA) system and a PrepLC 25-mm radial compression module. The column was equilibrated with 0.1% TFA in H_2O, and the eluent was 85% $MeCN$/15% H_2O with 0.086% TFA. A linear gradient from 20 to 90% over 30 min was used. The C-terminus of azurin with protected selenocysteine was a white solid (146 mg, 37%). A small amount of deselenated product was also recovered (12 mg). MALDI-MS M + 1 calcd 1973.2, found 1974.0; M + Na calcd 1995.2, found 1995.1; M + K calcd 2011.3, found 2012.0. The C-terminus peptide of azurin containing Cys112SeCys–Met121SeMet was prepared in the same way. MALDI-MS M + 1 calcd 2020.1, found 2019.8.

Selenocysteine Deprotection. Prior to use in the EPL reactions, the PMB–SeCys was deprotected by one of two possible procedures. The first procedure involved removal of the PMB protecting group with I_2 under acidic conditions. Iodine (5.4 mg, 0.02 mmol) was dissolved in a mixture of 8:1:1 acetic acid/H_2O:acetonitrile (0.8 mL). This solution was added to the protected peptide (10.4 mg, 0.005 mmol), and it was stirred under N_2 for 5 min. The solvent was then evaporated, and the resulting orange-brown oil was redissolved in 1:1 acetonitrile/H_2O and filtered through a syringe filter. The product was rapidly purified by one injection into a preparative RP-HPLC column. A white powder was isolated (7.5 mg, 77%). The product eluted as a single peak in the HPLC, but MALDI-MS data of the sample revealed a 3:2:1 mixture of deprotected selenol (M + 1 calcd 1853.1, found 1852.4)/diselenide dimer (M + 1 calcd 3703.3, found 3703.1)/monomer without selenium-(M + 1 calcd 1774.1, found 1772.3), consistent with previous reports.[22–24] A new technique for deprotection of the PMB-protected SeCys was later adopted for better yield of the desired product. Crude peptide was dissolved in 10 mL of 9:1 acetic acid/1 M HCl, and 1.1 equiv of 2-nitrobenzenesulfenyl chloride were added. The solution was stirred for 10 min. The solvent was evaporated, the peptide was dissolved in methanol, and the product was precipitated with cold Et_2O. The resulting white solid was isolated by filtration in a fine fritted filter, dissolved in a 1:1 mixture of $MeCN/H_2O$, and lyophilized. MALDI-MS analysis showed a 6:3:1 mixture of selenol monomer/Nps-selenosulfide/diselenide dimer. MALDI-MS for monomer, M + 1 is 1853.0 (calcd 1853.1), for Nps-selenosulfide, M + 1 is 2006.0 (calcd 2006.2), and for the diselenide dimer, M + 1 is 3703.4 (calcd 3704.2). This procedure resulted in significantly less deselenized product than the cleavage with I_2. This mixture was used in the EPL reaction.

Expressed Protein Ligation. The azurin–intein–chitin binding domain fusion protein was expressed in BLR(DE3) *Escherichia coli* (Novagen, Madison, WI). A 5 mL LB growth was started in a 37 °C

water bath. After 6–10 h, 2–4 flasks with 2 L of LB media were inoculated with 1 mL per flask of the 5 mL culture. The cultures were grown 11–12 h at 30 °C in an incubated shaker. IPTG was added to 0.3 mM, and induction was continued for 4 to 5 h. Cells were collected by centrifugation at 13 000*g* for 10 min, resuspended in 20 mM TrisHCl, pH 8.0, 500 mM NaCl, 1 mM EDTA, 1 mM PMSF, and 0.1% Triton X-100, and lysed with two passes through a French pressure cell. Inclusion bodies were denatured with a final concentration of 4 M urea. After centrifugation at 17 000*g* for 30 min, the supernatant was diluted with buffer (20 mM TrisHCl, pH 8.0, 500 mM NaCl) to a final concentration of 2 M urea, divided into three fractions, and passed down 3 × 6 mL chitin bead columns per 2 L of cell culture. The beads were washed with three column volumes of fresh urea buffer (20 mM TrisHCl, pH 8.0, 500 mM NaCl, 2 M urea), followed by six column volumes of buffer without urea. The cleavage buffer (20 mM TrisHCl, pH 8, 500 mM NaCl, 1 mM EDTA) was freeze/thaw degassed immediately prior to use. The cleavage buffer and 50 mM 2-mercaptoethanesulfonic acid (MESNA) or 50 mM *N*-methyl mercaptoacetamide (NMA) was added to the columns with 5–10 mg of the synthetic peptide (~1 mM). Reactions were allowed to proceed on the chitin column for 60 h at 4 °C. The proteins were eluted from the column and exchanged into 40 mM MOPS, pH 6.5, for purification with POROS 20 HQ anion-exchange resin (PerSeptive Biosystems, Cambridge, MA) on a BioCad Sprint HPLC system (PerSeptive Biosystems). Prior to purification, single equivalents of a 10 mM aqueous solution of $CuSO_4$ were added until saturation of the 677-nm peak. These coupling reactions with SeCys yielded less product than couplings with Cys. Typically, 0.1–0.25 mg of product per 6 mL of chitin beads (~0.5 L of cell culture) were obtained corresponding to a 2–6% yield. The products of the ligation reaction were analyzed by MALDI-MS (MESNA labeled-expressed azurin 1–111: calcd MW, 12 282; obsd 12 281 ± 6; SeCys ligation product, SeCys112-azurin hereafter: calcd MW, 13 993; obsd 13 991 ± 7). Electrospray ionization mass spectrometry (ESI-MS) of the blue protein after copper addition indicated a single copper bound to the SeCys112 azurin (calcd MW, 14 055; obsd 14 053 ± 7).

UV–Visible, MS, and EPR Spectroscopic Studies. UV–visible absorption spectra were collected at ambient temperature on a Varian CARY 3E spectrophotometer. ESI-MS and matrix-assisted laser desorption ionization mass spectrometry (MALDI-MS) were performed at the University of Illinois Mass Spectrometry Center. X-band EPR spectra were collected on a Varian E-122 spectrometer. The samples were run as frozen glasses at ~50 K using liquid He and an Air Products Helitran cryostat. Glycerol (30–50%) was used as a glassing agent. Q-band EPR spectra were collected on a Bruker E500-10 Elexsys system with a Q-band ER5106T TE011 cavity. Samples were run frozen at ~50 K with liquid He using an Oxford CF935 Cryostat controlled by an Oxford ITC-4 temperature controller. The magnetic fields were calibrated with a Varian NMR Gauss meter. W-band (94 GHz) spectra were obtained on the MARK II W-band EPR spectrometer[25] using a modulation amplitude of 3.0 G at 95 kHz. Samples were run as frozen glasses at 100 K in 0.57 mm i.d. tubes using an Oxford CF 1200 cryostat. The magnetic field calibration was obtained by use of a Metrolab PT 2025 NMR Gaussmeter, and the microwave frequency was measured with an EIP model 578 frequency counter equipped with a high-frequency option. All instruments were maintained by the University of Illinois EPR Research Center (IERC), University of Illinois at Urbana-Champaign. EPR spectra were simulated with the SIMPIPM program developed at the University of Illinois.[26] The program SIMPIPM includes strain-broadening effects calculated using exact gradients of the spin-Hamiltonian matrix. The program assumes that the strains in the system can be attributed to a Gaussian distribution

(22) Besse, D.; Moroder, L. *J. Pept. Sci.* **1997**, *3*, 442–453.
(23) Moroder, L.; Besse, D.; Musiol, H. J.; Rudolph-Bohner, S.; Siedler, F. *Biopolymers* **1996**, *40*, 207–234.
(24) Fiori, S.; Pegoraro, S.; Rudolph-Bohner, S.; Cramer, J.; Moroder, L. *Biopolymers* **2000**, *53*, 550–564.

(25) Nilges, M. J.; Smirnov, A. I.; Clarkson, R. B.; Belford, R. L. *Appl. Magn. Reson.* **1999**, *16*, 167–183.
(26) Nilges, M. J. *SIMPIPM*; Illinois EPR Research Center (IERC), University of Illinois: Urbana-Champain, 1979.

of the spin-Hamiltonian parameters and that, under the assumption that the variances in the spin-Hamiltonian parameters are small, the strain will give rise to Gaussian line broadening.

Extinction Coefficient Determination. The concentration of copper-(II) in the oxidized SeCys112 azurin sample was determined by quantification of the X-band EPR signal. The intensities of $CuSO_4$ under identical buffer conditions were used as the standard. The extinction coefficient can then be calculated from the absorption and concentration of copper(II) of the same sample.

Preparation of Dithionite Reduced Samples. The chemically reduced azurin EXAFS samples were prepared by titration with a 100 mM sodium dithionite stock. Equivalents were added to a ∼0.2 mM azurin solution on ice with stirring until the 677-nm band disappeared.

XAS Data Collection and Analysis. XAS data were collected at the Stanford Synchrotron Radiation Laboratory (SSRL) on beam lines 7.3 (BL 7.3) and 9.3 (BL 9.3) operating at 3.0 GeV with beam currents between 100 and 50 mA. Si220 monochromators with 1.2-mm slits were used to provide monochromatic radiation in the 8.8–9.7 (Cu K-edge) and 12.4–13.3 (Se K-edge) keV energy range. Harmonic rejection was achieved either by detuning the monochromator 50% at the end of the scan (BL 7.3, Cu and Se edges) or by means of a rhodium-coated mirror with a cutoff of 13 keV placed upstream of the monochromator (BL 9.3, Cu edges). The protein samples were measured as frozen glasses in 20–30% ethylene glycol at 11–14 K in fluorescence mode using either a 21-element (BL 7.3) or 30-element (BL 9.3) Canberra Ge detector. On BL 7.3 the count rate of each detector channel was kept below 110 kHz, while the rise in fluorescent counts through the edge was kept below 20 kHz per channel. Count rates were linear over this range, and no dead-time correction was necessary. For measurement of Cu XAS on BL 9.3, a Soller slit assembly fitted with a 6 μ Ni filter was used in conjunction with the 30-element detector to decrease the elastic scatter peak and protect against detector saturation. Here, maximum count rates per channel did not exceed 40 kHz. The summed data for each detector channel were then inspected, and only those channels that gave high-quality backgrounds free from glitches, drop outs, or diffraction peaks were included in the final average. Data reduction was performed as follows. First, a blank data file collected under identical conditions and detector geometry was subtracted from the summed experimental data. This procedure removed any residual K_β fluorescence from the Ni filter that was still present in the detector window and produced a flat preedge close to zero. Background subtraction was carried out in the PROCESS module of EXAFSPAK[27] using a Gaussian fit to the preedge region and a cubic spline fit with k^4 weighting in the postedge region. The E_0 (start of the EXAFS) was chosen as 9000 eV for Cu and 12 675 eV for Se. The EXAFS data were k^3-weighted and Fourier-transformed over the range $k = 0$–12.8 Å^{-1} (Cu) or $k = 0$–14 Å^{-1} (Se). Sequential scans were examined for radiation damage and/or photoreduction (as evidenced by edge shifts to lower energies), and only those scans with edge shifts less than 5% of the difference between the first scan of the series for the oxidized sample and a dithionite-reduced sample were included in the average used for EXAFS analysis. (Typically, oxidized samples began to exhibit measurable (>5%) shifts in edge position after ∼12 scans.) For analysis of absorption edges, more stringent criteria were employed. For each scan of a series, both the degree of photoreduction and the energy of the first inflection point of the copper calibration standard were examined, and only those scans free from both photoreduction edge shifts and <±0.1 eV calibration drift were included in the average.

Data analysis was performed using the OPT module of the EXAFSPAK computer suite.[27] Theoretical phase and amplitude functions were calculated using FEFF 8.0.[28] The EXAFS data were
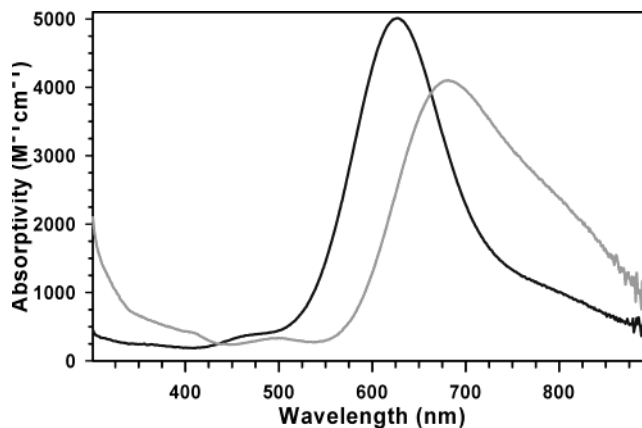

Figure 2. UV–visible absorption spectra for Sec112 azurin and WT azurin. The Sec112 derivative is less intense and shifted to lower energy.

simulated using a nonlinear Marquadt algorithm where the difference between experimental and the calculated data was minimized. For Cu edge data, coordination numbers were fixed at the crystallographically determined values for equatorial ligands, i.e., 2 N from histidine and 1 Se from selenocysteine. Contributions from axial ligands (for example Se in the Cys112SeCys–Met121SeMet derivative) were tested as to the importance of their contribution to the total EXAFS, again using the crystal structure of the WT enzyme as a starting model. For Se edges, the coordination number of the first shell C atoms was fixed at 1 for Cys112SeCys and 1.5 for Cys112SeCys–SeMet121, and contributions from the expected Se–Cu interactions were added as required. Variable parameters refined in the fit were as follows: ΔE_0 (a small energy correction at $k = 0$, depending on the oxidation state of the metal), R_i (the distance between the central absorber and atom i), and σ^2 (the Debye–Waller factor, defining the mean square deviation of R_i). EXAFS fits from derivatives of the same oxidation state and similar ligation are expected to exhibit very similar values of ΔE_0. When E_0 was allowed to float freely, small variations in E_0 were observed (±1.5 eV for oxidized samples, and ±3 eV for reduced samples). Since R and ΔE_0 are correlated, variability in E_0 can lead to lower precision in the determination of distances. Consequently, for distance comparisons between the derivatives of the same oxidation state, metrical parameters were refined using a fixed average value of ΔE_0. Multiple (double and triple) scattering pathways between the Cu absorber and the outer shell C scatterers of the imidazole ligands were calculated using FEFF and included if they exceeded 20% of the Cu–N(imidazole) single scattering intensity. A goodness-of-fit (F_w) parameter, displayed at the end of each cycle, was used to determine the merit of the fit. F_w is defined as follows:

$$F_w = \sum_{i=1}^{n} \frac{k^6(\text{Data} - \text{Model})^2}{k^6(\text{Data})^2}$$

Results

The UV–visible absorption spectra of Cu(II)-containing WT azurin and SeCys112 azurin are shown in Figure 2. As reported previously, the visible spectrum of WT azurin is dominated by a strong absorption at ∼628 nm, due to a S(Cys112) $3p_\pi \rightarrow$ Cu(II) $3d_{xy}$ charge-transfer (CT) transition.[29-32] In addition, weaker absorption bands at 366, 466, and ∼800 nm are observed and have been assigned to Met a_1 and His π_1 to Cu(II) $3d_{xy}$ CT transitions and Cu(II) d → d transitions, respectively. Interest-

(27) George, G. N. *EXAFSPAK*; Stanford Synchrotron Radiation Laboratory: Menlo Park, CA, 1995.
(28) Ankudinov, A. L.; Ravel, B.; Rehr, J. J.; Conradson, S. D. *Phys. Rev. B* **1998**, 7565–7576.
(29) Solomon, E. I.; Baldwin, M. J.; Lowery, M. L. *Chem. Rev.* **1992**, *92*, 1–542.
(30) Penfield, K. W.; Gewirth, A. A.; Solomon, E. I. *J. Am. Chem. Soc.* **1985**, *107*, 4519–4529.
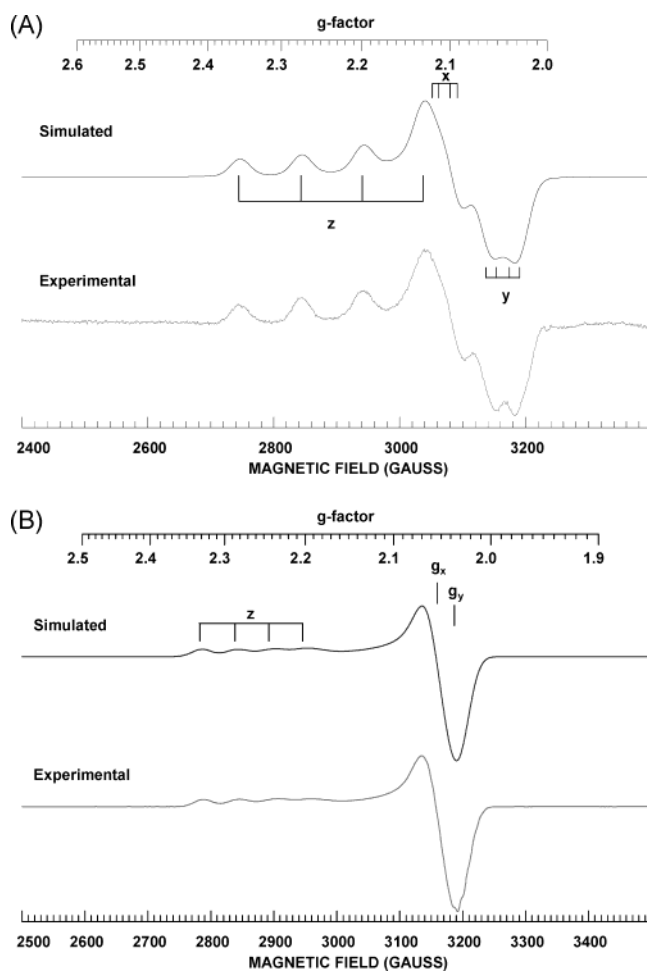(31) Gewirth, A. A.; Solomon, E. I. *J. Am. Chem. Soc.* **1988**, *110*, 3811–3819.

(A)

(B)

Figure 3. Experimental and simulated X-band EPR spectra for (A) SeCys112 azurin and (B) WT azurin. X-band experimental conditions: microwave frequency, 9.089 GHz; microwave power, 0.2 mW; modulation amplitude, 5 G; time constant, 32 ms; sweep time, 60 s; number of scans, 20; temperature, 20 K.

(A)

(B)

Figure 4. Experimental and simulated Q-band EPR spectra for (A) SeCys112 azurin and (B) WT azurin. Q-band experimental conditions: microwave frequency, 34.156 GHz; microwave power, 2 mW; modulation amplitude, 4 G; time constant, 40.96 ms; sweep time, 42 s; number of scans, 20; temperature, 100 K.

ingly, the visible absorption spectrum of SeCys112 azurin is similar to that of WT azurin, with the absorption bands red-shifted.

The X-band EPR spectra of SeCys112 azurin and WT azurin are shown in Figure 3, while the corresponding Q-band EPR spectra are shown in Figure 4. The EPR parameters obtained from multifrequency spectral simulation are given in Table 1 for WT azurin and SeCys112, respectively. The values obtained for WT azurin are similar to those reported previously.[33] The values of g are better determined here because of inclusion of the Q-band spectrum in the fitting routine. For the Euler angles,[34] the value of β (the angle of noncoincidence between the z-direction of the hyperfine and g-tensors) is quite close to that reported previously, but the value of α differs significantly.

(32) We are using the standard coordinate system which corresponds to D_{2d} symmetry: (a) Pierloot, K.; De Kerpel, J. O. A.; Ryde, U.; Roos, B. O. *J. Am. Chem. Soc.* **1997**, *119*, 218−226. (b) Börger, B.; Gutschank, J.; Suter, D.; Thomson, A. J.; Bingham, S. J. *J. Am. Chem. Soc.* **2001**, *123*, 2334−2339. (c) van Gastel, M.; Coremans, J. W. A.; Sommerdijk, H.; van Hemert, M. C.; Groenen, E. J. *J. Am. Chem. Soc.* **2002**, *124*, 2035−2041. The nonstandard coordinate system used by Solomon et al. has the x and y axes rotated by 45°: (d) Solomon, E. I.; Hare, J. W.; Dooley, D. M.; Dawson, J. H.; Stephens, P. J.; Gray, H. B. *J. Am. Chem. Soc.* **1980**, *102*, 168−178
(33) Antholine, W. E.; Hanna, P. M.; McMillin, D. *Biophys. J.* **1993**, *64*, 267−272.
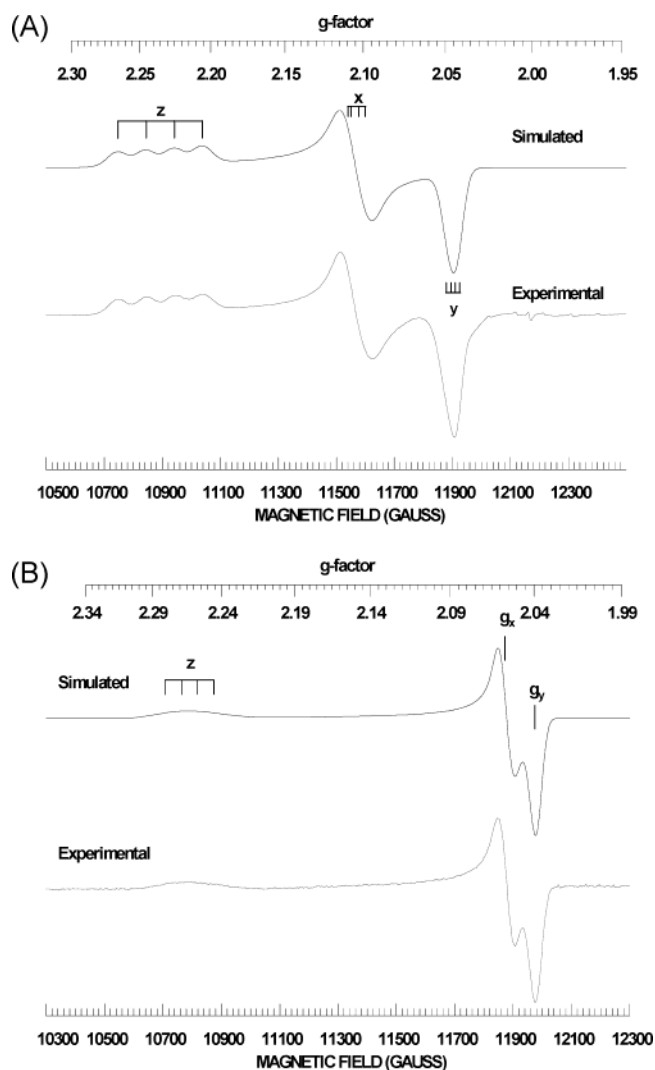(34) Rose, M. E. *Elementary Theory of Angular Momentum*; Wiley: New York, 1957.

Because of the approximately axial nature of the EPR spectrum, the value of α, as well as that of γ, has only a weak effect on the EPR spectrum, and as such this result is not unexpected.

SeCys112 and WT azurin show marked differences in both the values of the g and hyperfine tensors. Particularly, SeCys112 azurin displays a much larger parallel hyperfine splitting of 100 G ($A_{||} = -310.0$ MHz) than the 56 G for WT ($A_{||} = -178.2$ MHz) as is readily seen in Figure 3. Also seen are a much more rhombic g-tensor, which is plainly evident from the higher frequency Q-band EPR spectra (Figure 4) and W-band EPR spectra (not shown), and the results of EPR simulations that give g-values of 2.2354, 2.1056, and 2.0448 (compared with 2.2640, 2.0564, and 2.0390 for WT azurin).

Another marked difference between SeCys112 and WT azurin is that the g- and A-strain along the z-direction for SeCys112 azurin is half that of the WT form. This is clearly seen in the X-band spectra of SeCys112 and WT azurin (Figure 3). Whereas WT azurin shows a clear m_I dependent line width along the z-direction turning points, SeCys112 azurin does not. (The differences in the values of g- and A-strain for the x- and y-directions are not as pronounced, nor does the strain in these

Table 1[a]

EPR Spin Hamiltonian and Strain Parameters for WT Azurin				EPR Spin Hamiltonian and Strain Parameters for SeCys112 Azurin[a]			
g_x	2.0564	σg_x	0.0027 [+0.028]	g_x	2.1056	σg_x	0.0058 [+0.056]
g_y	2.0390	σg_y	0.0019 [+0.045]	g_y	2.0458	σg_y	0.0029 [+0.067]
g_z	2.2640	σg_z	0.0173 [+0.062]	g_z	2.2354	σg_z	0.0075 [+0.032]
A_x[b]	−13.4	σA_x	nm nm	A_x[b]	−24.8	σA_x	nm nm
A_y	−26.6	σA_y	nm nm	A_y	−53.4	σA_y	nm nm
A_z	−178.2	σA_z	11.9 [−0.067]	A_z	−310.0	σA_z	−0.9 [+0.003]
α_{gA}[c]	+7.8°			α_{gA}[c]	+4.3		
β_{gA}	+9.7°			β_{gA}	+10.2		
γ_{gA}	+10.8°			γ_{gA}	−40.5		
QD[b]	+7.8			QD[b]	+15.7		
QE	+0			QE	+1.2		
W_x[d]	29.5			W_x[d]	25.4		
W_y	30.4			W_y	27.3		
W_z	18.5			W_z	24.3		

[a] Hyperfine principal values in MHz. (For units of 10^{-4} cm^{-1}, divide by 3.) Fractional strain is given in square brackets (for g, $\Delta(\Delta g)/\Delta g$ is given); the sign in front of the variance in the principal values of g and A represents the correlation coefficient of ± 1.0; nm = not measured. [b] Hyperfine and nuclear quadrupole values represent the weighted average of both Cu^{63} and Cu^{65} naturally occurring isotopes. [c] Euler angles (convention of Rose[34]) relating the noncoincidence between g and A (nuclear quadrupole tensor is assumed coincident with A). [d] Residual line width (Gaussian) in Gauss.
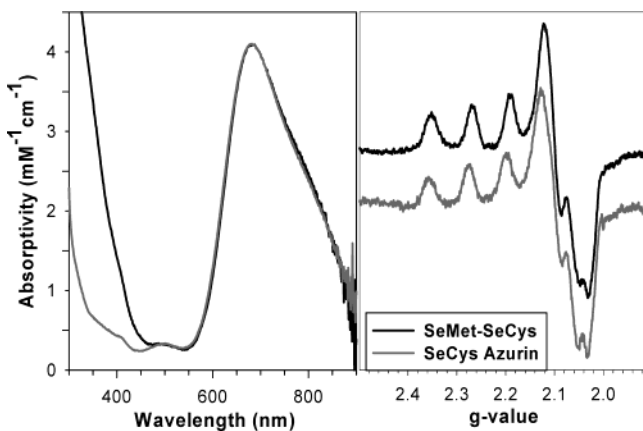

Figure 5. UV−visible absorption (left) and X-band EPR (right) spectra of the SeCys112SeMet121 azurin variant (top) compared with SeCys112 azurin (bottom). Experimental EPR conditions: microwave frequency, 9.088 GHz; microwave power, 20 mW; modulation amplitude, 2 G; time constant, 32 ms; sweep time, 60 s; number of scans, 20; temperature, 30 K.

directions give a clear m_I-dependent line width, as the hyperfine splittings are either not resolved or only partially resolved.) The residual Gaussian line width of 20−30 G arises from unresolved nitrogen superhyperfine structure from the two histidine ligands and the β protons of the Cys112 ligand, and in the case of WT azurin these splittings have been determined previously.[33] Unlike the WT azurin which clearly shows partially resolved superhyperfine structure in the second-harmonic X-band spectrum, the SeCys112 azurin does not. As such, the nitrogen and proton superhyperfine couplings were neglected in the simulations, since the difference in couplings between WT and SeCys112 azurin cannot be determined from the spectra presented here.

A mixed selenolate selenoether copper(II) complex was prepared by mutation of the axial methionine ligand to a selenomethionine in the SeCys112 azurin construct. Both selenium-modified amino acids were incorporated through the synthetic 17 amino acid peptide. The UV−visible absorption and X-band EPR spectra of the SeMet−SeCys azurin variant are much like the SeCys variant (Figure 5). The UV−visible absorption spectra displays around a 2-nm red-shift of the Se to Cu(II) charge-transfer band. For the X-band EPR spectra (Figure 5), the parallel hyperfine coupling splitting is 102 G, about 2 G more than that of the SeCys azurin, and the $g_{\parallel}$ value is a slightly lower value (2.230 vs 2.235 for SeCys azurin),
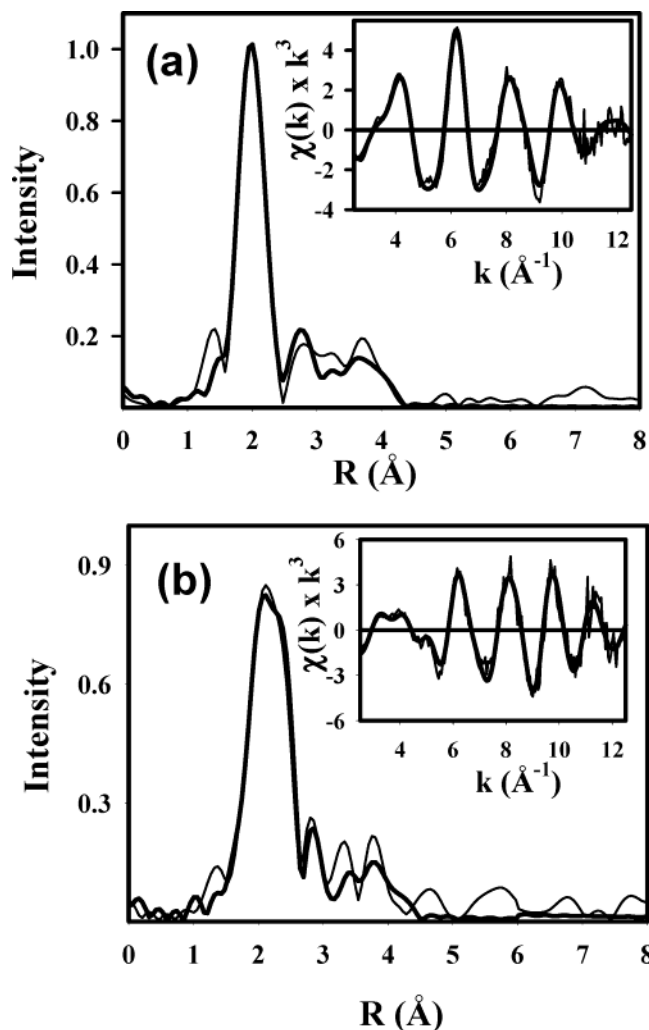

Figure 6. Comparison of EXAFS data of EPL-synthesized WT and SeCys112 azurin. Copper edge experimental and simulated Fourier transforms and EXAFS (inset) for (a) oxidized WT and (b) oxidized SeCys112 azurin. Thin lines are experimental data; thick lines are simulated data. The parameters used in the simulations are given in Table 2 and Berry et al.[20]

which suggests a very small delocalization onto the SeMet Se compared to the SeCys Se.

Figure 6 compares the Cu K EXAFS spectrum of the oxidized derivative of SeCys112 azurin with the WT azurin produced by EPL. The most striking differences are the broadening of

Table 2. EXAFS Fitting Parameters for SeCys112 and SeCys112/SeMet121 *P. aeruginosa* Azurin

	Copper EXAFS				Selenium EXAFS				
sample	scatterer (coord. no.)	distance (Å)	Debye–Waller (Å²)	$-E_0$ (eV)	F	scatterer	distance (Å)	Debye–Waller (Å²)	$-E_0$ (eV)	F
SeCys112 oxidized	2 N(imid)	1.97(2)	0.005	7.46	0.34	2 C	1.94(2)	0.002	11.37	0.32
	1 Se	2.30(2)	0.005			1 Cu	2.31(2)	0.005		
	4 C2/C5(imid) single scatt.	2.97	0.007			2 C	3.53	0.006		
	8 C2/C5(imid) mult. scatt.	3.20	0.008							
	8 C3/N4(imid) mult. scatt.	4.22	0.011							
SeCys112 reduced	2 N(imid)	2.00(2)	0.001	7.51	0.29	2 C	1.94(2)	0.002	10.16	0.37
	1 Se	2.33(2)	0.003			0.66 Cu	2.32(2)	0.003		
	4 C2/C5(imid) single scatt.	3.02	0.003			2 C	3.46	0.009		
	8 C2/C5(imid) mult. scatt.	3.18	0.008							
	8 C3/N4(imid) mult. scatt.	4.23	0.009							
SeCys112/SeM121 oxidized	2 N(imid)	2.00(2)	0.004	7.46	0.29	1.5 C	1.93(2)	0.003	11.70	0.37
	1 Se	2.32(2)	0.004			0.5 Cu	2.35(2)	0.005		
	4 C2/C5(imid) single scatt.	3.01	0.009							
	8 C2/C5(imid) mult. scatt.	3.20	0.008							
	8 C3/N4(imid) mult. scatt.	4.22	0.011							

the first peak of the FT to higher *R* values with indications of a splitting of the shell into two components, strong oscillations in the EXAFS which maximize at $k \approx 9$ Å, and the appearance of well-resolved structure in the EXAFS in the $k = 3-5$ Å. These spectral attributes are characteristic of the replacement of S with Se and have their physical origin as follows. First, the increase in the Cu–Se bond length, together with the increased scattering amplitude of Se over S, causes the first shell transform peak to split into Cu–N and Cu–Se components. Second, the intense EXAFS oscillations due to Cu–Se scattering maximize at higher *k* ($k = \sim 9$ Å^{-1}) than those from S, in line with the expected shift in the maximum of the amplitude envelope for the heavier Se atom. Third, the shift of the Se scattering to higher *k* allows the structure associated with imidazole outer-shell multiple scattering to become better resolved in the $k = 3-5$ Å^{-1} region.

Figure 6 shows a simulation of the spectrum, which includes EXAFS contributions (single and multiple scattering) from two imidazole groups and a Se atom. The Cu–N(imid) distance is 1.97 Å, somewhat longer than that (1.92 Å) found for WT (S–Cys) azurin. The Cu–Se distance is 2.30 ± 0.02 Å as compared to 2.15 ± 0.01 Å for the S-derivative. This represents an increase of 0.14 Å, which is close to the increase in covalent radius of Se over S. The fit nicely reproduces both the increase in amplitude due to Se scattering maximizing at $k = 9$ Å^{-1} and the low *k* structure due to the imidazole multiple scattering. Attempts to include a Cu–S(Met) or Cu–O(Gly) interaction at $R = 2.5-3.5$ Å produced no improvement in either the qualitative or quantitative goodness of fit. This is in line with recent studies at the Se edge of a Met121SeMet derivative, which showed no observable Se–Cu scattering due to the coordinated methionine residue.[20] The parameters used in the fit are given in Table 2.

Figure 7 shows the best fit obtained for the reduced (Cu(I)-containing) SeCys112 derivative. Inspection shows that the
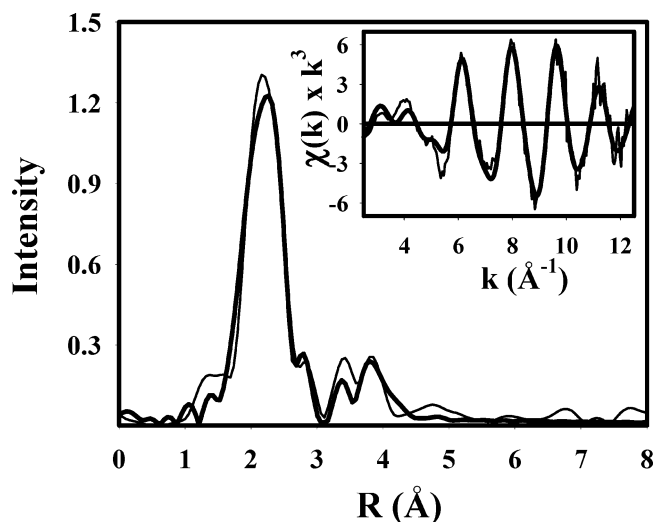

Figure 7. Copper edge experimental and simulated Fourier transforms and EXAFS (inset) for reduced SeCys112 azurin. Thin lines are experimental data; thick lines are simulated data. The parameters used in the simulations are given in Table 2.

spectrum is very similar to that of the oxidized protein. This is borne out by the simulation results which indicate a slight lengthening of the Cu–N and Cu–Se shells to 2.00 ± 0.02 Å and 2.33 ± 0.02 Å, respectively. Both distances increase less than typically observed for reduction of Cu–cysteinate cupredoxin derivatives.[20,35]

The great utility of selenocysteine as a spectroscopic probe lies in the accessibility of the Se K-edge and its associated EXAFS, which in turn provides a ligand-centered view of the structure at the metal center. Accordingly, we carried out Se K-edge measurements on both the oxidized and reduced

(35) DeBeer George, S.; Basumallick, L.; Szilagyi, R. K.; Randall, D. W.; Hill, M. G.; Nersissian, A. M.; Valentine, J. S.; Hedman, B.; Hodgson, K. O.; Solomon, E. I. *J. Am. Chem. Soc.* **2003**, *125*, 11314–11328.
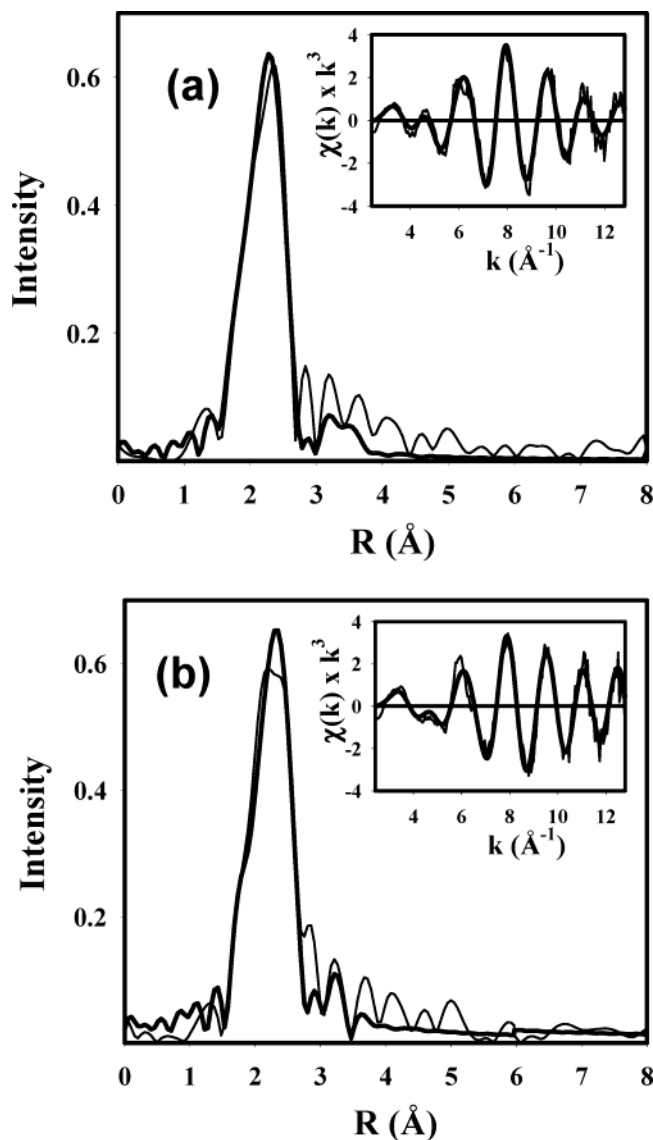
Figure 8. Selenium edge experimental and simulated Fourier transforms and EXAFS (inset) for (a) oxidized and (b) reduced SeCys112 azurin. Thin lines are experimental data; thick lines are simulated data. The parameters used in the simulations are given in Table 2.

SeCys112 derivatives. The spectra and their associated simulations are shown in Figure 8 with parameters used in the fitting process given in Table 2. The Se K-EXAFS data look quite similar to their Cu counterparts, again exhibiting a FT composed of a split first shell (Se–C, Se–Cu), with EXAFS dominated by a strong oscillation maximizing at $k = 8-9$ Å^{-1} due to Se–Cu scattering. When considering the Se-derived structural parameters, it is expected that Se–Cu distances and their respective Debye–Waller terms should mirror those found at the Cu edge. This was indeed the case, where values of R_{Se-Cu} of 2.31 and 2.32 ± 0.02 Å were found for oxidized and reduced proteins, respectively. The Se–C distance was 1.94 Å in both derivatives. However, Se–Cu coordination numbers (CN) may be significantly different, because decreased copper site occupancy can reduce the Se–Cu coordination below unity. The simulations therefore fixed the Cu–Se DW factor at the value found from simulating the copper edge data and refined the CN. Using this procedure, the oxidized derivative was found to have a Se–Cu coordination number of 1, indicating full copper site

occupancy. However, for the reduced protein, a Se–Cu coordination number of 0.66 was found. When the reduced data were simulated using a Se–Cu CN of unity, much poorer fits were obtained. Some additional Se low-Z intensity around 3.5 Å was necessary to reproduce the structure in the EXAFS in the $k = 3-5$ Å^{-1} region. A Se K-edge study of the diselenide selenocystine revealed similar (but less intense) features in this region (data not shown). We conclude that these C atoms represent single scattering contributions from more distant shells of low-Z scatterers within the selenocysteine residue.

The near identical Cu–Se distances in the oxidized and reduced SeCys112 proteins are remarkable and differ significantly from the situation in S-containing derivatives where reduction leads up to a 0.08 Å increase in the Cu–S distance.[35,36] This may suggest that the larger Se atom restricts the ability of the site to accommodate redox-induced changes in bond length more than the S homologue. Alternatively, it may reflect altered electronic structural properties at the copper center since the cupredoxin site exhibits some degree of plasticity to accommodate conservative mutations or metals with different coordination preferences.[37] To further probe the structural consequences of the Cys112SeCys substitution, we studied an oxidized double mutant with the S atoms of the Cys112 and Met121 residues each substituted with a Se atom. Here, the Cu edge has the potential to show Cu–Se scattering due to both the Cu–Cys and Cu–Met interactions, while the Se edge should show the average of the Se–C and Se–Cu interactions of the Cys and Met residues, respectively. The results are shown in Figure 9. The Cu edge data appear qualitatively similar to the single Cys112SeCys mutant data, and simulation shows only minor differences, viz. a 0.02 Å lengthening of the Cu–Se bond to 2.32 ± 0.02 Å and a 0.03 Å lengthening of the Cu–histidine shell to 2.00 ± 0.02 Å. Of particular significance, no evidence of scattering from the Cu–SeMet interaction was observed, suggesting that like the Met121SeMet single mutant,[20] this is a very weak bond. At Se, we observe 1.5 Se–C interactions at 1.93 ± 0.02 Å and 0.5 Cu at 2.35 ± 0.02 Å. Inclusion of additional Se–Cu scattering due to the methionine–copper interaction did not improve the fit significantly. These results show that the structure of the copper center appears to be little influenced by Se substitution at the coordinating M112 residue. Thus, the structural/electronic determinants of the azurin site are localized within the Cu–His$_2$Cys triad.

Figure 10 compares the X-ray absorption near edge (XANES) region for the oxidized and reduced single mutants at the Cu and Se edges. The copper edges show the expected shift to lower energy on reduction. The oxidized SeCys112 derivative exhibits a low-intensity (1s → 3d) transition at 8979 eV similar to WT (also shown in Figure 10 for comparison). In addition, three weak shoulders are observed on the rising edge at 8983.1, 8986.6, and 8992.7 eV. These transitions mirror similar peaks on the absorption edge of the WT azurin but are more intense and slightly shifted to lower the energy. The 8983 eV transition is usually assigned to a 1s → 4p + ligand-to-metal charge transfer (shakedown) transition.[35,38] Both the increase in intensity and the slight shift to lower binding energy observed in the

(36) Cheung, K. C.; Strange, R. W.; Hasnain, S. S. *Acta Crystallogr., Sect. D* **2000**, *56* (Pt 6), 697–704.
(37) Bonander, N.; Vanngard, T.; Tsai, L. C.; Langer, V.; Nar, H.; Sjolin, L. *Proteins: Struct., Funct., Genet.* **1997**, *27*, 385–394.
(38) Kau, L. S.; Spira-Solomon, D.; Penner-Hahn, J. E.; Hodgson, K. O.; Solomon, E. I. *J. Am. Chem. Soc.* **1987**, *109*, 6433–6422.
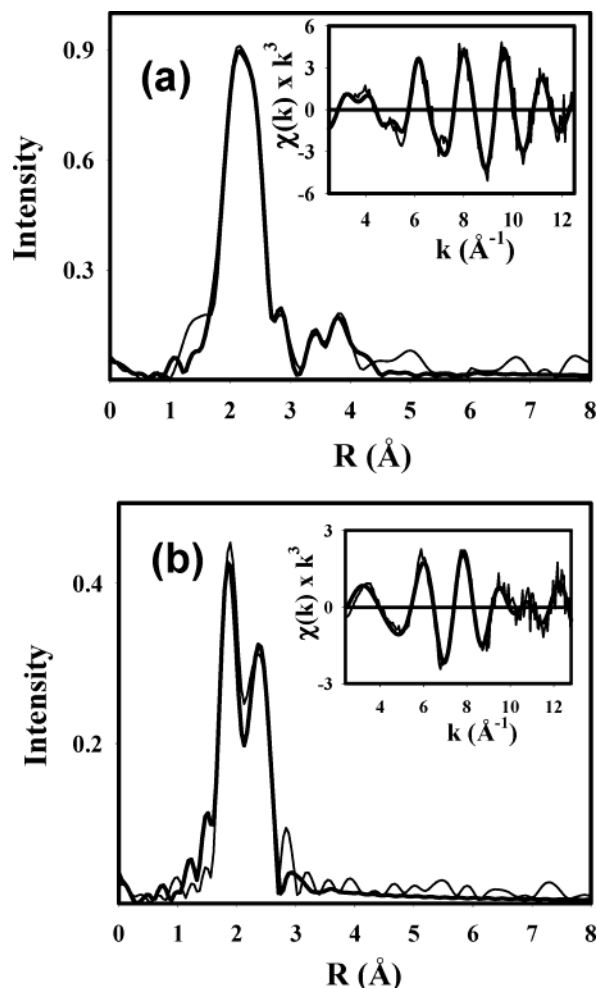
Figure 9. Experimental and simulated Fourier transforms and EXAFS (inset) for (a) copper edge and (b) selenium edge for the SeCys112SeMet121 azurin double mutant. Thin lines are experimental data; thick lines are simulated data. The parameters used in the simulations are given in Table 2.

SeCys112 oxidized edge suggests an increase in electronic charge density at copper due to greater electron donation from the softer more polarizable Se atom. Increased intensity of the 8983 eV LMCT + shakedown peak has also been observed in the Q99M mutant of stellacyanin relative to the WT protein, where substitution of S(Met) for the native Gln99 O-ligand is proposed to weaken the axial interaction and lead to increased covalency of the Cu−S (cys) bond.[35] However, it should be noted that these effects are small, and other spectral features of the SeCys112 azurin predict the opposite trend (vide infra). The copper edge of the reduced derivative shows peaks at 8983.0, 8986.6, and 8992.7 eV at similar energies but with larger intensities than the oxidized derivative. The 8983 eV peak is not as intense as often observed in three-coordinate Cu(I) complexes, but is similar to that observed in other reduced cupredoxins.[35,39]

Selenium K-edges of oxidized and reduced SeCys112 azurin are shown in Figure 10b. Two peaks are observed: a shoulder at 12 661.1 eV in both derivatives and a main peak at 12 665.0 eV (oxidized) and 12 665.6 eV (reduced). These features closely
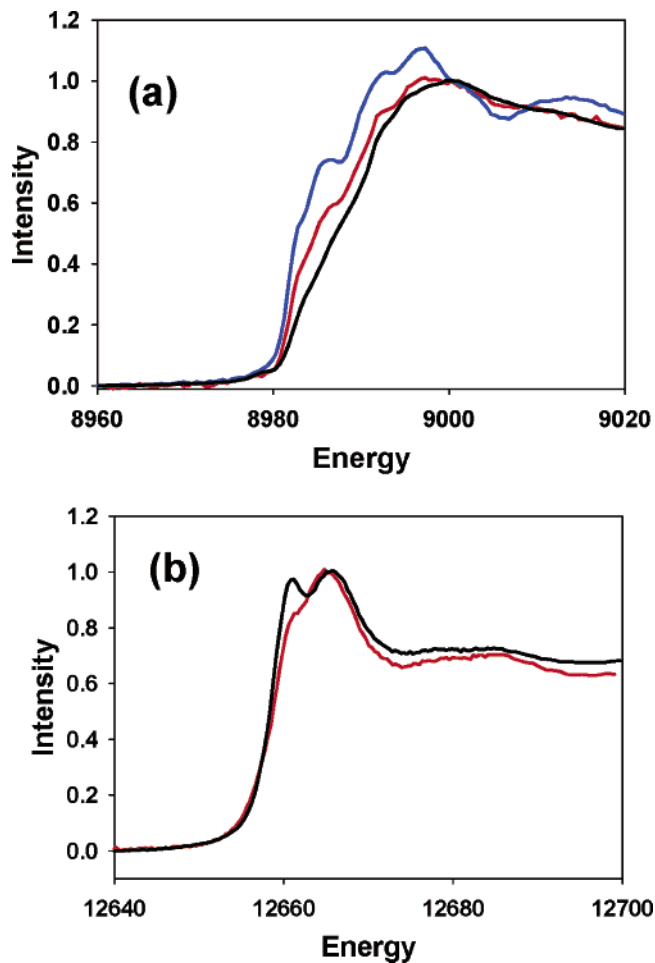
(39) DeBeer, S.; Wittung-Stafshede, P.; Leckner, J.; Karlsson, G.; Winkler, J. R.; Gray, H. B.; Malmstrom, B. G.; Solomon, E. I.; Hedman, B.; Hodgson, K. O. *Inorg. Chim. Acta* **2000**, *297*, 278−282.

Figure 10. Comparison of absorption edges for oxidized and reduced SeCys112 azurin and WT azurin. (a) Cu edges. From left to right: reduced SeCys112, oxidized SeCys112, and oxidized WT. (b) Se edges. Red line oxidized; black line reduced. Copper edge spectra were normalized at 9000 eV, while selenium edge spectra were normalized at 12 665.5 eV.

resemble those of the Se K-edges of the free selenocysteine amino acid.[40] The 12 661.1 eV peak in the oxidized protein is almost identical to that reported for the deprotonated selenocysteinate ion, while in the reduced protein the intensity has increased, more closely resembling that reported for the protonated selenocysteine amino acid.[40] The difference in intensity for this peak may be related to oxidation state, but more likely reflects the lower site occupancy of the reduced selenocysteine derivative already inferred from EXAFS analysis, where absence of the metal ion could lead to protonation of the residue within the active site.

Discussion

Using the expressed protein ligation protocol, we have prepared a semisynthetic derivative of azurin in which the copper-binding Cys112 residue has been replaced with selenocysteine. The advantages of this substitution are twofold. First, it represents a highly conservative substitution which is predicted to produce only minor perturbation on the geometric and electronic structure of the cupredoxin copper center, allowing subtle effects on redox potential and electronic structure to be investigated. Because of the unique nature of the Cu−S(cys)

(40) Pickering, I. J.; George, G. N.; Fleet-Stalder, V.; Chasteen, T. G.; Prince, R. G. *J. Biol. Inorg. Chem.* **1999**, *4*, 791−794.

interactions in cupredoxins with their associated high covalency, mutation to other residues has generally led to dramatic structural and electronic perturbations at the copper center, eliminating the type 1 nature of the site.[41–43] Second, it introduces a ligand-centered spectroscopic probe for structure determination using X-ray absorption spectroscopy. In this way, the derivative serves as a paradigm for Cys to SeCys substitutions in other systems where the ability to correlate XAS studies at both Cu and Se K-edges promises to provide a wealth of structural and electronic information. However, we stress that in the absence of a crystal structure, structural and electronic comparisons must be approached with caution.

Most copper–selenium complexes involve the Cu(I) oxidation state, which is readily explained in simplistic terms by the more favorable covalent interactions possible between the soft Cu(I) ion and the electron-rich more polarizable selenium center. The oxidized form of SeCys112 azurin is therefore unique in that it represents the first example of a Cu(II)–selenolate complex. The visible absorption spectrum is similar to that of WT azurin, with the absorption bands red-shifted. The most intense transition at 677 nm can be assigned to the Se → Cu(II) CT band. The red-shift of this band from 628 nm in the Cys112 (WT) protein is consistent with the lower ionization energy of selenium. Other peaks located at 408 and 498 nm can be tentatively assigned to red-shifted Met and His → Cu CT bands, respectively. In addition, the intensity of the 677-nm peak is lower than that of the WT 625-nm peak. The SeCys112 derivative also shows altered EPR parameters, with increased and more rhombic g-values. The small $A_{||}$, which is a characteristic feature of blue copper sites (and attributed to the highly covalent Cu–S(cys) interaction in cupredoxins), is not observed. These features may suggest that contrary to simplistic arguments, the Cu(II)–SeCys112 azurin is actually slightly less covalent than its Cu–S counterpart. However, complexities in the analysis of the spectral data have made it difficult to assess the level of covalency in SeCys112 azurin.

The Cu–Se bond length derived from EXAFS was found to be 2.30 ± 0.02 Å, which is 0.14 ±.02 Å longer than the Cu–S distance in WT azurin.[20,36,44,45] This is close to the difference in covalent radii of S and Se (0.135 Å, covalent radii taken as half the X–X bond length, X = S, Se), suggesting that the difference in bond length can be attributed almost entirely to the larger Se atom. The Cu–S bond length in WT azurin is short relative to Cu–S distances found in the majority of three-coordinate mixed CuN_2S complexes and is generally accepted as being the result of the presence of significant covalency within a trigonally distorted Cu(II) center. The large percentage of Cu–S covalency (38, 41, and 45% in plastocyanin, stellacyanin, and azurin, respectively) has been proposed as a driving force for a specific electron-transfer pathway through the cysteine ligand.[35,46–48] An important question is thus whether

the Cu–Se bond is similarly short in SeCys112 azurin, and if so, whether this in turn directs electron transfer through the Cu–SeCys pathway.

The chemistry of copper with selenides, selenolates, and selenoethers is sparse, and predominately involves the Cu(I) oxidation state. As stated above, few if any Cu(II) selenolate complexes have been described in the literature. The coordination chemistry of selenolates and selenides is predominately polynuclear, with both terminal and bridging Se atoms present in the structures.[49–56] Cu(II) selenoether complexes are known, but tend toward demetalation and formation of diselenide bonds.[57–59] From this limited literature, trends in Cu(I)–Se distances can be discerned, with Cu(I)–selenide and –selenolate bond lengths ranging from 2.3–2.45 Å and Cu(I)–selenoether bond lengths in the range 2.40–2.55 Å. Thus, both the Cu(II)–Se (2.30 Å) and the Cu(I)–Se (2.32 Å) are within the range for Cu(I) selenolates, but very close to the lower end.

Interactions between exogenous selenolate ligands and metal centers in proteins provide additional information without the complication of multinuclear selenium complexation. Selenophenol binds to an iron center in the Mo–Fe protein of nitrogenase with an Fe–Se bond length of 2.41 Å.[60] Seleno-homocysteine binds to Zn in methionine synthase with a Zn–Se bond length of 2.43 Å.[5] The crystal structure of formate dehydrogenase shows the Se atom of the selenocysteine ligand ∼2.7 Å from the Mo center, considerably longer than the distances of Se to first-row transition metals described above.[61] These examples may suggest that metal selenolate distances for first-row transition metals in mononuclear environments should be closer to 2.4 Å. If true, this would imply that the measured Cu–Se distances in Cys112SeCys azurin are indeed short like their Cu–S homologues. The reduced Cu(I) ion is known to form more stable complexes with selenolates such that a stronger Se–Cu(I) interaction would be expected. These factors could explain the observed smaller differences in oxidized and reduced Cu–Se bond lengths relative to the Cu–S(cysteine) derivatives.

The electronic structure of blue copper centers has been studied in considerable detail using a variety of experimental and theoretical techniques. The short Cu–S bond has been described in terms of a $S(\pi)$–$Cu(d_{xy})$ interaction where the lobes

(41) Faham, S.; Mizoguchi, T. J.; Adman, E. T.; Gray, H. B.; Richards, J. H.; Rees, D. C. *J. Biol. Inorg. Chem.* **1997**, *2*, 464−469.
(42) DeBeer, S.; Kiser, C. N.; Mines, G. A.; Richards, J. H.; Gray, H. B.; Solomon, E. I.; Hedman, B.; Hodgson, K. O. *Inorg. Chem.* **1999**, *38*, 433−438.
(43) Mizoguchi, T. J.; Dibilio, A. J.; Gray, H. B.; Richards, J. H. *J. Am. Chem. Soc.* **1992**, *114*, 10076−10078.
(44) Libeu, C. A.; Kukimoto, M.; Nishiyama, M.; Horinouchi, S.; Adman, E. T. *Biochemistry* **1997**, *36*, 13160−13179.
(45) Gray, H. B.; Malmstrom, B. G.; Williams, R. J. *J. Biol. Inorg. Chem.* **2000**, *5*, 551−559.
(46) Shadle, S. E.; Penner-Hahn, J. E.; Schugar, H. J.; Hedman, B.; Hodgson, K. O.; Solomon, E. I. *J. Am. Chem. Soc.* **1993**, *115*, 767−776.
(47) DeBeer George, S.; Metz, M.; Szilagyi, R. K.; Wang, H.; Cramer, S. P.; Lu, V.; Tolman, W. B.; Hedman, B.; Hodgson, K. O.; Solomon, E. I. *J. Am. Chem. Soc.* **2001**, *123*, 5757−5767.
(48) Glaser, T.; Hedman, B.; Hodgson, K. O.; Solomon, E. I. *Acc. Chem. Res.* **2000**, *33*, 859−868.
(49) Christuk, C. C.; Ansari, M. A.; Ibers, J. A. *Inorg. Chem.* **1992**, *31*, 4365−4369.
(50) Cheng, Y.; Emge, T. J.; Brennan, J. G. *Inorg. Chem.* **1996**, *35*, 7339−7344.
(51) Yam, V. W.-W.; Lo, K. K.-W.; Cheung, K.-K. *Inorg. Chem.* **1996**, *35*, 3459−3462.
(52) Salm, R. J.; Ibers, J. A. *Inorg. Chem.* **1994**, *33*, 4216−4220.
(53) Raymond, C. C.; Dorhout, P. K. *Inorg. Chem.* **1996**, *35*, 5634−5641.
(54) Hong, M.; Zhang, Q.; Cao, R.; Wu, D.; Chen, J.; Zhang, W.; Liu, H.; Lu, J. *Inorg. Chem.* **1997**, *36*, 6251−6260.
(55) Yam, V. W.; Lam, C. H.; Fung, W. K.; Cheung, K. K. *Inorg. Chem.* **2001**, *40*, 3435−3442.
(56) Yam, V. W.-W.; Lam, C.-H.; Cheung, K.-K. *Chem. Commun.* **2001**, 545−546.
(57) Batchelor, R. J.; Einstein, F. W. B.; Gay, I. D.; Gu, J.-H.; Pinto, M.; Zhou, X.-M. *J. Am. Chem. Soc.* **1990**, *112*, 3706−3707.
(58) Batchelor, R. J.; Einstein, F. W. B.; Gay, I. D.; Gu, J.-H.; Pinto, B. M. *J. Organomet. Chem.* **1991**, *411*, 376.
(59) Black, J. R.; Champness, N. R.; Levason, W.; Reid, G. *Inorg. Chem.* **1996**, *35*, 1820−1824.
(60) Conradson, S. D.; Burgess, B. K.; Newton, W. E.; Di Cicco, A.; Filipponi, A.; Wu, Z. Y.; Natoli, C. R.; Hedman, B.; Hodgson, K. O. *Proc. Natl. Acad. Sci. U.S.A.* **1994**, *91*, 1290−1293.
(61) Boyington, J. C.; Gladyshev, V. N.; Khangulov, S. V.; Stadtman, T. C.; Sun, P. D. *Science* **1997**, *275*, 1305−1308.

of the Cu(d_{xy}) HOMO bisect the Cu−S vector, resulting in what is essentially a metal−S π-bond with about 40% S covalency.[46] The half occupancy of the antibonding HOMO in the oxidized protein serves to shorten the Cu−S distance relative to the reduced protein.[62] This electronic interaction manifests itself by the presence of a well-resolved preedge peak in the sulfur K-edge spectra due to covalent mixing of S and metal orbitals in the HOMO.[35,46−48] It is of interest to note that no such preedge feature is resolvable in the Se K-edge spectra, which raises the question as to whether the selenocysteine ligand shares the high covalency of the Cu−S homologue.

The EPR spectrum of the oxidized SeCys112 azurin has an $A_{\parallel}$ value of 100 G, roughly double that of WT azurin, which from a preliminary analysis was thought to imply less covalent character.[19] It is possible that the increased value of $A_{\parallel}$ relative to the WT protein could be attributed to a reduction in covalency arising from changes in either (a) the geometry of the active site or (b) the Cu−Se orbital overlap. While these effects could lead to an increase in both the spin density at the copper and the rhombic character of the g-tensor, it is more likely that changes in the spin−orbit couplings (SOC) are responsible for the observed differences in EPR parameters for SeCys112 and WT azurin.

The marked increase in rhombic character of the g-tensor of SeCys112 azurin is most likely the result of the large SOC for selenium. While sulfur has an SOC of 382 cm^{-1}, selenium has an SOC of 1690 cm^{-1}. Not only is the SOC of Se more than four times that of S, but it is also about twice that of Cu (828 cm^{-1}).[63] Thus, the SOC of Se is expected to make a major contribution to the g-tensor for SeCys112 azurin. Since the SOC arises primarily from the Cu and Se atoms, Δg_{pq}, the *pq*-component of the tensor representing the shift from the free electron value, g_e, can be approximated when the smaller multicentered terms are neglected:[64]

$$\Delta g_{pq} \approx -2\lambda_{Cu}\sum_{i\neq 0}\frac{<\chi_0^{Cu}|L_0^{Cu}|\chi_i^{Cu}|><\chi_i^{Cu}|L_q^{Cu}|\chi_0^{Cu}>}{\epsilon_i - \epsilon_0}$$
$$-2\lambda_{Se}\sum_{i\neq 0}\frac{<\chi_0^{Se}|L_0^{Se}|\chi_i^{Se}|><\chi_i^{Se}|L_q^{Se}|\chi_0^{Se}>}{\epsilon_i - \epsilon_0} \quad (1)$$

where λ_{Cu} and λ_{Se} are the SOC for Cu and Se, respectively; L_q^{Cu} and L_q^{Se} are the *q*th component of the angular momentum vector, centered on the Cu and Se nucleus, respectively; χ_i^{Cu} and χ_i^{Se} are the part of the *i*th MO that is centered on Cu and Se, respectively; and ϵ_0 and ϵ_i are the ground-state and excited-state orbital energies, respectively. The ground-state orbital containing the unpaired spin (HOMO) is expected to be an antibonding combination of the Cu $3d_{xy}$ and the Se $3p\pi$ (p_y; the *x*-direction being oriented approximately along the Cu−Se bond) orbital with significant delocalization of the electron on both Cu and Se atoms:

$$\Psi_0 \approx c_0|Cu\ 3d_{xy} > -d_0|Se\ 3p_y> \quad (2)$$

Using this expression, assuming that the *x*-direction is oriented along the Cu−Se bond and neglecting overlap, the above

expression for *g* can be further simplified:

$$\Delta g_z \approx +8\lambda_{Cu}\sum_i\frac{c_0^2 c_i[Cu\ d_{x^2-y^2}]^2}{\epsilon_0 - \epsilon_i} + 2\lambda_{Se}\sum_i\frac{d_0^2 d_i[Se\ p_x]^2}{\epsilon_0 - \epsilon_i} \quad (3)$$

$$\Delta g_y \approx +2\lambda_{Cu}\sum_i\frac{c_0^2 c_i[Cu\ d_{yz}]^2}{\epsilon_0 - \epsilon_i} \quad (4)$$

$$\Delta g_y \approx +2\lambda_{Cu}\sum_i\frac{c_0^2 c_i[Cu\ d_{xz}]^2}{\epsilon_0 - \epsilon_i} + 2\lambda_{Se}\sum_i\frac{d_0^2 c_i[Se\ p_z]^2}{\epsilon_0 - \epsilon_i} \quad (5)$$

where c_i [Cu $d_{x^2-y^2}$], c_i [Cu d_{xz}] and c_i [Cu d_{yz}] are the coefficients of the |Cu $d_{x^2-y^2}$>, |Cu d_{xz}>, and |Cu d_{yz}> orbital terms, respectively, and d_i [Se p_x] and d_i [Se p_z] are the coefficients of the |Se p_x> and |Se p_z> orbital terms in the *i*th excited state. Thus, the unpaired electron in the p_π or p_y orbital will mix via Se SOC primarily with excited states having spin density in Se p orbitals orthogonal to the p_y, namely p_x and p_z, and the Se SOC will contribute in first-order to g_x and g_z but not to g_y. Thus, the larger of the two in-plane g-values, 2.1056, can be assigned to g_x. Such an argument has been presented for the rhombicity of the g-tensor of plastocyanin,[30] where calculations showed that 88% of the rhombic splitting was due to S SOC. Thus, for SeCys112 azurin with its much larger SOC than that for Se, the large rhombic splitting between g_x and g_y can be almost entirely attributed to the Se SOC. Just as the Se SOC gives a large contribution to g_x, so is a contribution of similar magnitude expected for g_z. In the limit of perfect sp^2 hybridization around the Se atom, the contribution to g_z should be equal to that of g_x. Thus, in the absence of Se SOC (leaving essentially Cu SOC only), the g-tensor should be nearly axial (with g_x and g_y both equal to around 2.045) and g_z somewhere in the vicinity of 2.18.

The other major difference in EPR parameters between SeCys112 and WT azurin is that $A_{\parallel}$ for SeCys112 azurin is 70% larger than that for WT azurin. While one could attribute this increase to a greater spin density on the Cu and less delocalization onto the Se, the actual change in delocalization is expected to be small. Dialkyldithiocarbamato−copper complexes and their selenium analogues have been well-studied by EPR and their ground-state properties have been well-characterized.[65−67] Delocalization on the selenium carbamate is found to be 29% larger than that for the analogous sulfur complex, which corresponds to an increase of 7% per Se atom. For azurin there is only one sulfur atom, and unlike the dithio- or diselenocarbamate complexes which have the lobes of the ground-state Cu d_{xy} orbital pointing directly at the four sulfur or selenium atoms, the lobes of the Cu ground-state d-orbital (d_{xy}) point away from the S or Se atom forming a π-bond. As such, a relatively small increase in delocalization for SeCys112 azurin should be expected.

The Cu hyperfine can be broken up into three components:[68] the isotropic Fermi contact term which depends not only on

(62) Gukert, J. A.; Lowery, M. D.; Solomon, E. I. *J. Am. Chem. Soc.* **1995**, *117*, 2817−2844.
(63) Clementi, E. *IBM J. Res. Dev.* **1965**, *9*, 2−3.
(64) Stone, A. J. *Proc. R. Soc. London, Ser. A* **1963**, *271*, 424−434.

(65) Keijzers, C. P.; De Vries, H. J. M.; Van der Avoird, A. *Inorg. Chem.* **1972**, *6*, 1338−1343.
(66) Keijzers, C. P.; Paulussen, G. F. M.; De Boer, E. *Mol. Phys.* **1975**, *4*, 973−1006.
(67) Keijzers, C. P.; De Boer, E. *Mol. Phys.* **1975**, *4*, 1007−1020.
(68) McGarvey, B. R. *Transition Met. Chem.* **1966**, *3*, 89.

the spin density in the Cu d$_{xy}$ orbital but also on spin polarization of other orbitals, the anisotropic spin dipolar terms which to first-order are directly dependent upon the spin-density in the Cu d$_{xy}$ orbital and direct mixture of spin-density in Cu s orbitals, and finally the orbital terms which depend not only on the Cu spin density but mainly upon SOC mixing of excited states, particularly d-states.

$$A_{zz} = -P_d\kappa_0\alpha^2 - \frac{4}{7}P_d\alpha^2 + P_d\left[\Delta g_{zz} + \frac{3}{14}\Delta g_{xx} + \frac{3}{14}\Delta g_{yy}\right]$$
(6)

$$A_{yy} = -P_d\kappa_0\alpha^2 + \frac{2}{7}P_d\alpha^2 + P_d\left[\Delta g_{yy} + \frac{3}{14}\Delta g_{xx}\right]$$
(7)

$$A_{xx} = -P_d\kappa_0\alpha^2 - \frac{2}{7}P_d\alpha^2 + P_d\left[\Delta g_{xx} + \frac{3}{14}\Delta g_{yy}\right]$$
(8)

where α^2 $(= c_0^2)$ represents the spin population of the Cu d$_{xy}$ orbital, P_d is equal to $g_e\beta_e g_N\beta_N/\langle r^3\rangle_d$ or 1188 MHz [30] for Cu, and κ_0 is the indirect Fermi contact term for a single electron in a 3d$_{xy}$ orbital. In eqs 6–8, the first term represents the isotropic Fermi contact splitting, which is positive; the second term is the spin dipolar term, which is positive for A_{zz} and negative for A_{xx} and A_{yy}; and the third term represents the orbital contributions which will all be positive, since the g-shifts are all positive for Cu in azurin. For A_{zz}, the orbital term is of similar magnitude and opposite sign as the other two put together, and as such, an unusually low value of A can occur due to near cancellation as occurs in WT azurin. Thus, the large value of $A_{||}$ for SeCys112 azurin may not be due to an increase in spin density on the Cu but rather changes in SOC mixing, which would lower the orbital contributions to A and give a disproportionately large change in A. A good example of this is the EPR spectrum of the high symmetry form (D_{4h}) CuCl$_2$ compared to its low symmetry form (D_{2d}). Even though the D_{2d} site has 6% more spin density on the Cu, its absolute value for $A_{||}$ is much smaller than that for the D_{4h} site (75 vs 492 MHz).[69] The much smaller value of $A_{||}$ of the D_{2d} form is attributed primarily to a nearly 200% increase (300 MHz) in the orbital part of A for the D_{2d} form, and as such masks any change in the spin dipolar part of A which is the best measure of changes in spin density on the Cu.

Provided that the g-tensor is determined primarily by the Cu SOC, the orbital part of $A_{||}$ can be approximated directly from the observed g tensor. While this may be true to some extent for WT azurin, it is definitely not true for SeCys112 azurin because of the large contribution to g from the Se SOC. However, for SeCys112 azurin, the value of $g_{||}$, considering only SOC of the Cu, was estimated to be around 2.18 (vide supra). From this value, we can estimate that the orbital part of $A_{||}$ (which is positive in sign) will be 100 MHz smaller than that for SeCys112 azurin, and this would then account for 75% of the difference for $A_{||}$ between SeCys112 and WT azurin. Thus, the large difference in the parallel hyperfine between SeCys112 and WT azurin can also be accounted for primarily by SOC effects: namely, a decrease in the energy between spin−orbit-coupled d-states (d$_{xy}$ vs d$_{x^2-y^2}$), giving rise to a smaller parallel g-shift for SeCys112 azurin with a resultant decrease in the orbital part of $A_{||}$. (A similar case is seen for glutamine mutants of stellacyanin.)[35]

The smaller g- and A-strains observed for SeCys112 azurin could be attributed to the SeCys112 azurin having a better-defined or more rigid structure around the copper atom. However, the fact that this decrease is seen particularly along the z-direction and that the g- and A-strains are highly correlated (ϵ_{gA}, the correlation coefficient between the g and A values ≈ 1.0)[70] would suggest that the smaller strain in SeCys112 azurin can also be attributed to changes in SOC arising from a decrease in the energy between spin−orbit-coupled d-states (d$_{xy}$ vs d$_{x^2-y^2}$), resulting in both a smaller value of $g_{||}$ and a proportionately smaller spread in g values due to strain. In conclusion, the large difference in the hyperfine and g-tensor components of Se-Cys112 and WT azurin can be accounted for by SOC effects, either by the larger SOC for Se or by a decrease in the energy between spin−orbit-coupled d-states (d$_{xy}$ vs d$_{x^2-y^2}$). As such, the dominance of SOC effects in the EPR spectra mask contributions from changes in covalency.

Altered interactions with an axial ligand could also signal changes in site geometry or electronic structure. WT azurin has two more distant ligands, Met121 and Gly45, at distances in excess of 3 Å from the copper.[20,36,44,71] We therefore examined a double mutant in which both Cys112 and Met121 were replaced by SeCys and SeMet residues, respectively. Similar to the SeMet121 derivative of WT azurin, the SeMet121 derivative of SeCys112 azurin did not appreciably perturb the copper site spectroscopic characteristics. The UV−visible absorption spectrum displays around a 2-nm red-shift of the Se to Cu(II) charge-transfer band. This is a very similar change to that observed in the incorporation of SeMet121 in WT azurin, where only a 3-nm shift in the S to Cu(II) charge-transfer band was observed.[20] For the X-band EPR spectra, the parallel hyperfine coupling constant is 102 G, about 2 G more than that of the SeCys112 azurin, and the $g_{||}$ value is slightly lower (2.230 vs 2.234 for SeCys112 azurin). Similar changes were observed in the SeMet121 variant of WT azurin in which the hyperfine coupling constant decreased slightly (3 G), and the $g_{||}$ value is slightly lowered. This derivative showed almost unchanged metrical parameters for the Cu−His$_2$Cys triad with at most a 0.02 Å lengthening of the Cu−N(His) and Cu−Se(Cys) distances and a single Se−Cu interaction at 2.32 from 0.5 Se atoms in the Se edge data. No evidence for any Se−Cu scattering from the SeMet121 ligand was found. This mirrors our recent finding for a SeMet121 single mutant where the absence of any Se−Cu scattering indicated that the axial interaction from selenomethionine does not strengthen appreciably through the substitution of Se in either oxidized or reduced forms.[20] No data are available for the reduced double mutant.

The reduction potential of SeCys112 azurin (316 mV) was reported to be somewhat less than WT azurin (328 mV). Given the strong stabilization of Cu(I) by selenolates and selenoethers in low molecular weight complexes, the decrease in reduction potential is surprising. The near equivalence of Cu(II)− and Cu(I)−Se bond lengths in SeCys112 azurin may suggest that the Cu(II)−Se interaction is less strong than its Cu−S counterpart in WT, perhaps due to a decrease in covalency which could offset any stabilization of Cu(I) by the softer Se ligand.

(69) Gerwith, A. A.; Cohen, S. L.; Schugar, H. J.; Solomon, E. I. *Inorg. Chem.* **1987**, *26*, 1133−1146.

(70) Froncisz, W.; Hyde, J. S. *J. Chem. Phys.* **1980**, *73*, 3123−3131.
(71) Karlsson, B. G.; Tsai, L. C.; Nar, H.; Sanders-Loehr, J.; Bonander, N.; Langer, V.; Sjolin, L. *Biochemistry* **1997**, *36*, 4089−4095.

In conclusion, we have used UV−vis, EPR, and Cu and Se K-XAS to characterize the SeCys112 derivative of *P. aeruginosa* azurin, and we report the first Cu−Se distances for a seleno-cysteine derivative of a copper protein. This study demonstrates the utility of EPL as a strategy for the selective incorporation of selenocysteine into the active sites of metalloproteins, making possible both metal and ligand K-EXAFS studies.